GSA DATA REPOSITORY 2015057

BONINITIC MELT INCLUSIONS IN CHROME SPINEL FROM THE OGASAWARA ARCHIPELAGO

DATA REPOSITORY for "Thermal and chemical evolution of the subarc mantle revealed by spinel-hosted melt inclusions in boninite from the Ogasawara (Bonin) Archipelago" by Susumu Umino, Keitaro Kitamura, Kyoko Kanayama, Akihiro Tamura, Naoya Sakamoto, Osamu Ishizuka, and Shoji Arai.

Analytical methods and procedures

Chrome spinels were handpicked under binocular after cleaning and sieving the sand samples with pure water. Spinel crystals embedded in epoxy resin on a slide glass were ground and polished to expose the core of crystals with melt inclusions, which were utilized for major and trace element analyses, including H_2O (Table DR-1).

Major elements of glass and minerals were analyzed by a JEOL JXA-8800 electron probe microanalyzer (EPMA) at Kanazawa University. The accelerating voltage was 15 kV and the specimen current was 12 nA. Analyses of glass followed the procedures of Noguchi *et al*. (2004) using broad beam diameters <30 μm. The corrections were made according to ZAF method. Relative errors (1σ) of melt inclusion analyses are better than 0.4% for SiO_2, 11.3% for TiO_2, 1.3% for Al_2O_3, 3.0% for FeO, 23.3% for MnO, 1.2% for MgO, 1.7% for CaO, 7.8% for Na_2O, 7.9% for K_2O and 6.7% for Cr_2O_3.

Trace element compositions (REEs, V, Cr, Co, Ni, Li, B, Sc, Rb, Sr, Y, Zr, Nb, Cs, Ba, Hf, Ta, Pb, Th and U) of glass were analyzed by laser ablation (193 nm ArF excimer: MicroLas GeoLas Q-plus) inductively coupled plasma mass spectrometry (Agilent 7500s) (LA-ICP-MS) at Kanazawa University (Morishita et al., 2005a, b). Each analysis was performed by ablating spots of 30 or 40 μm in diameter at 5 Hz with energy density of 8 J/cm^2 per pulse. Signal integration times were 50 seconds for a gas background interval and 50 seconds for an ablation interval. BCR-2G (USGS glass reference material) was used as the primary calibration standard and its element concentration values are selected from the GeoReM database (see Jochum and Nohl., 2008). Repeated analyses of NIST 610, NIST612 and BIR show that reproducibility is better than ±11% (1 σ)

except B, Cs, Ta and U (Table DR-2). Data reduction was facilitated using ^{29}Si as internal standards for glass, based on SiO_2 contents obtained by EPMA analysis, and followed a protocol essentially identical to that outlined by Longerich et al. (1996). Details of the analytical method and data quality for the LA-ICP-MS system at Kanazawa University are described in Morishita et al. (2005a, b) and Ichiyama et al. (2013).

H_2O concentrations in glass of melt inclusions were determined by using a Secondary Ion Mass Spectrometry (SIMS) Cameca IMS-6F of the Creative Research Institution, Hokkaido University. Analytical procedures followed Miyagi and Yurimoto (1995) using natural hornblende with 1.66 wt% H_2O as a standard. Water contents (in wt%) were determined by comparing $^{1}H/^{30}Si$ ratios of unknown samples with averages of those of the standard hornblende measured on the same day.

Water content

H_2O contents vary from 1 to 5 wt% and H_2O/Ce ratios from 2000 to 43200. Interstitial glass in melt inclusions consisting mainly of variolitic pyroxene crystals and vesicles (Fig. 1D) tends to show lower H_2O concentrations (<2.4 wt%). These glass inclusions have consistently lower H_2O/Ce ratios compared to glass in melt inclusions comprising pure glass and a few shrinkage vesicles of the same geochemical type (Fig. DR-4). H_2O and Ce do not fractionate during partial melting of the source mantle and fractional crystallization of magmas due to their similar partition coefficients between melt and relevant mineral phases (Michael, 1995; Hauri et al., 2006), and hence melt inclusions of the same geochemical type are expected to have similar H_2O/Ce ratios. Thus, the coincidence of the variolitic texture and the lower H_2O contents and H_2O/Ce ratios compared to those of pure glass inclusions of the same geochemical type suggests that the variolitic melt inclusions experienced degassing and partially lost their original water during ascent to the surface. We therefore have corrected water contents of degassed samples and estimated the original water contents based on Ce contents, by assuming the original H_2O/Ce ratios of the degassed samples to be equal to the average H_2O/Ce ratio of undegassed samples of the same geochemical type. Because all low-Si-F (flat chondrite-normalized REE pattern) inclusions show a variolitic texture with low H_2O/Ce ratios, the original H_2O/Ce ratio of the type was assumed to be 9800, the maximum ratio among Type F inclusions observed. This gives the minimum

estimates of the original H_2O contents for low-Si-F inclusions. The restored H_2O contents range from 1 to 6 wt% with restored H_2O/Ce ratios varying from 9800 to 43200.

Procedure of T-P estimate of olivine-orthopyroxene multiple saturation

T-P estimates for the primary boninitic magmas to be multiply saturated with olivine and orthopyroxene were determined by solving simultaneously the olivine-liquid geothermobarometry (equation (4) of Putirka et al., 2007) and olivine-orthopyroxene-liquid geothermobarometry (equation (42) of Putirka, 2008), following the procedure described in Putirka (2008). Major element compositions including Fe_2O_3, and H_2O contents are used as input. First, (1) The Fe^{3+}/Fe^{2+} ratio at prescribed f_{O2} (here $\Delta\log(FMQ) = 0$ to +2) and the liquidus temperature is determined by using alphaMELTS (Smith and Asimow, 2005) at initial guess of pressure. (2) T and P obtained from the geothermobarometry are then used to calculate Fe^{3+}/Fe^{2+} ratio at prescribed f_{O2} by alphaMELTS. (1) and (2) are repeated iteratively until T, P, and Fe^{3+}/Fe^{2+} ratio become stable within 0.5%. Varying f_{O2} by 2 in log unit brings a little difference in T-P estimates compared to the uncertainty inherited from the geothermobarometry, while increase in H_2O content by 1 wt% reduces the estimated T and P by 34°C and 0.17 GPa, respectively.

REFERENCES

Falloon, T.J., and Danyushevsky, L.V., 2000, Melting of refractory mantle at 1.5, 2 and 2.5 GPa under anhydrous and H2O-saturated conditions: Implications for the petrogenesis of high-Ca boninites and the influence of subduction components on mantle melting: Journal of Petrology, v. 41, p. 257–283.

Hauri, E.H., Gaetani, G.A., and Green, T.H., 2006, Partitioning of water during melting of the Earth's upper mantle at H_2O-undersaturated conditions: Earth and Planetary Science Letters, v. 248, 715–734.

Ichiyama, Y., Morishita, T., Tamura, A., and Arai, S., 2013, Petrology of peridotite xenolith-bearing basaltic to andesitic lavas from the Shiribeshi Seamount, off northwestern Hokkaido, the Sea of Japan: Journal of Asian Earth Sciences, v. 76, p. 48–58.

Jochum, K. P., and Nohl, U., 2008, Reference materials in geochemistry and environmental research and the GeoReM database: Chemical Geology, v. 253, p. 50–53.

Longerich, H.P., Jackson, S.E. and Gunther, D., 1996, Laser ablation inductively coupled plasma mass spectrometric transient signal data acquisition and analyte concentration calculation: Journal of Analytical Atomic Spectrometry, v. 11, p. 899–904.

Michael, P., 1995, Regionally distinctive sources of depleted MORB: Evidence from trace elements and H_2O: Earth and Planetary Science Letters, v. 131, p. 301–320.

Miyagi, I., and Yurimoto, H., 1995, Water content of melt inclusions in phenocrysts using Secondary Ion Mass Spectrometer: Bulletin of Volcanological Society of Japan, v. 40, p. 349–355.

Morishita, T., Ishida, Y., and Arai, S., 2005a, Simultaneous determination of multiple trace element compositions in thin (<30 μm) layers of BCR-2G by 193 nm ArF excimer laser ablation-ICP-MS: implications for matrix effect and elemental fractionation on quantitative analysis: Geochemical Journal, v. 39, p. 327–40.

Morishita, T., Ishida, Y., Arai, S., and Shirasaka, M., 2005b, Determination of multiple trace element compositions in thin (30 μm) layers of NIST SRM 614 and 616 using laser ablation-inductively coupled plasma-mass spectrometry (LA-ICP-MS): Geostandrand and Geoanalytical Research, v. 29, p. 107-122.

Noguchi, S., Morishita, T., and Toramaru, A., 2004, Corrections for Na-loss on micro-analysis of glasses by electron probe X-ray micro analyzer (in Japanese with English abstract): Japanese Magazine of Mineralogical and Petrological Sciences, v. 33, p. 85–95.

Smith, P.M., and Asimow, P.D., 2005, Adiabat_1ph: A new public front-end to the MELTS, pMELTS, and pHMELTS models: Geochemistry, Geophysics, Geosystems, v. 6, Q02004, doi:10.1029/2004GC000816.

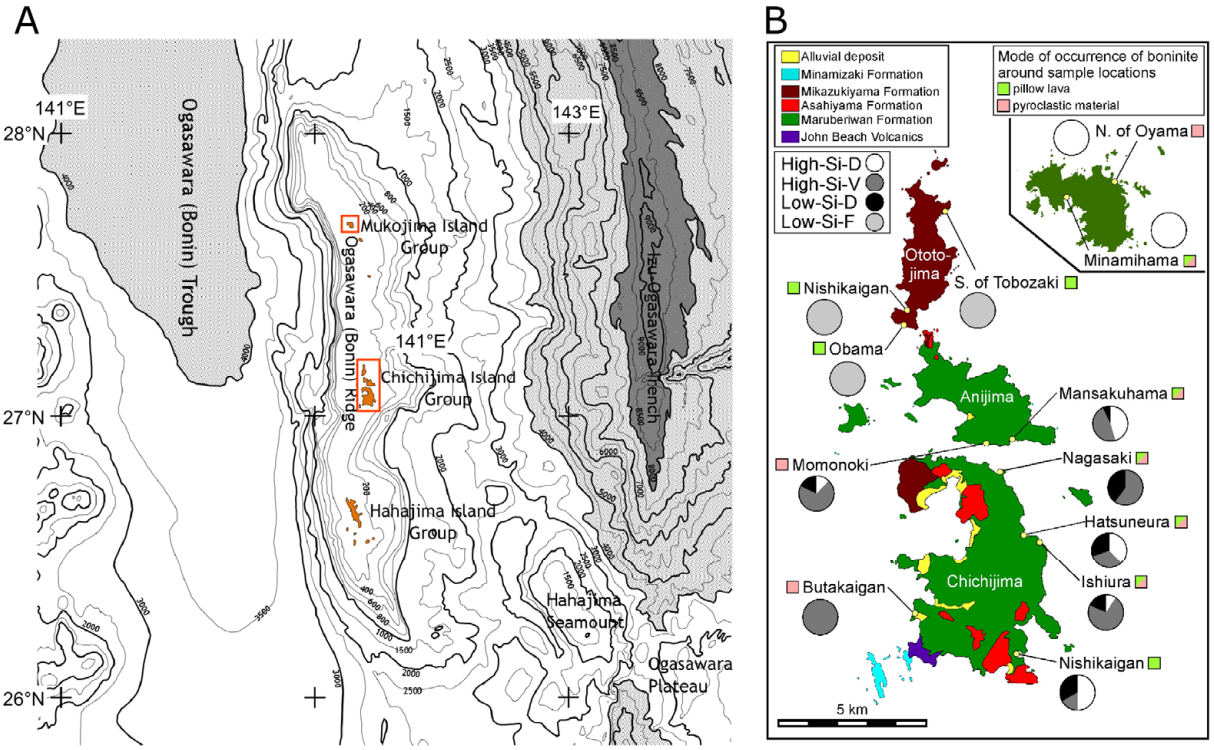

Figure DR-1. Locations of the Ogasawara Archipelago (A) and samples of chrome spinel together with the mode of occurrence of the host rocks and geochemical types (B).

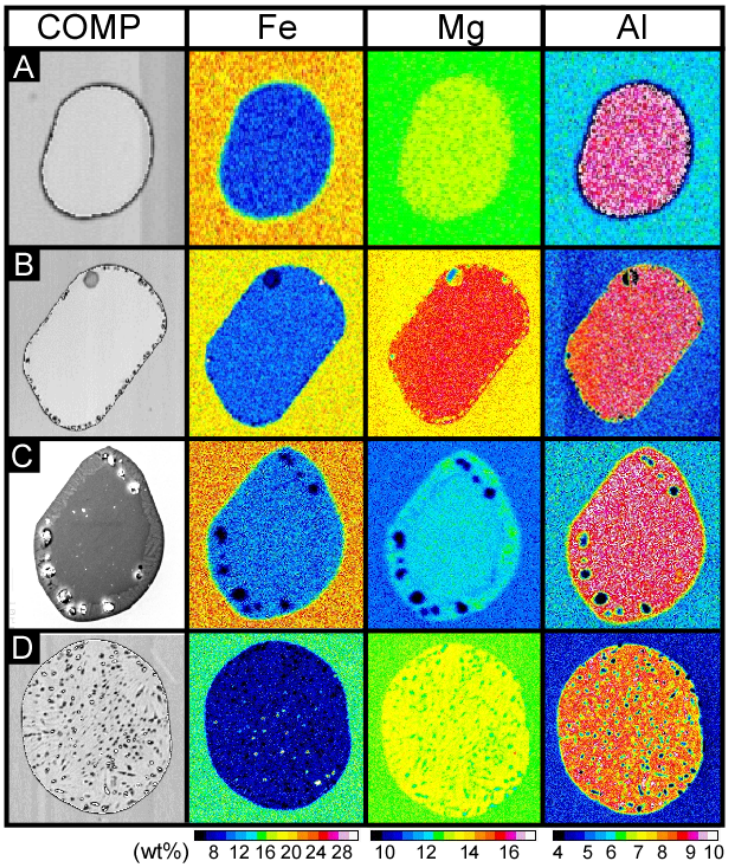

Figure DR-2. SEM (COMPO) images (left) and pseudo-colored EMPA maps (right) of Fe, Mg, and Al of melt inclusions and the host chrome spinel shown in Figure 1. Note the absence of Fe-rich and Mg-poor halos in the spinel host adjacent to the melt inclusions, confirming the absence of diffusive Fe-loss from the melt.

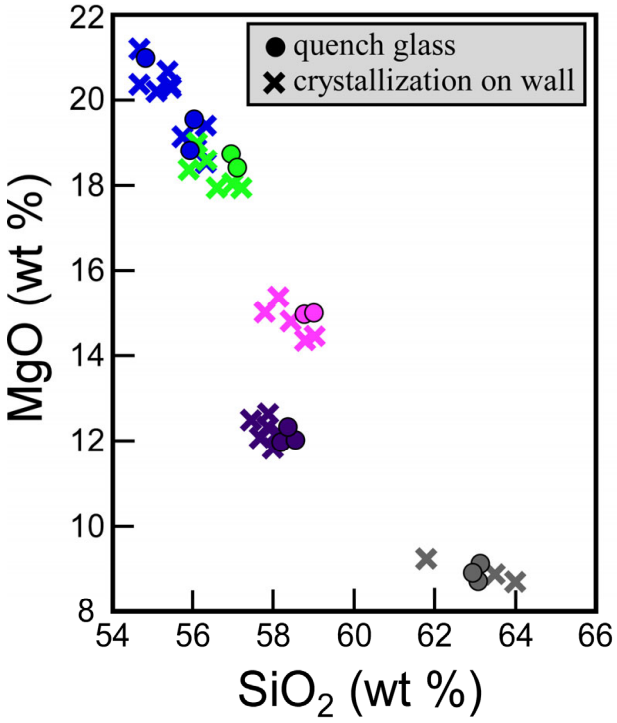

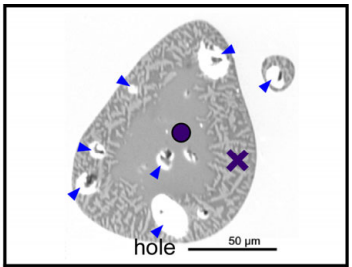

Point	●	✖
SiO_2	58.38	57.83
TiO_2	0.07	0.10
Al_2O_3	8.83	8.85
FeO*	11.45	11.57
MnO	0.29	0.23
MgO	12.08	12.17
CaO	6.61	6.71
Na_2O	1.35	1.10
K_2O	0.34	0.38
Cr_2O_3	0.60	1.09

Figure DR-3. Analyses of melt inclusions (left) composed of the central glass pool (dots) surrounded by an outer zone with quench crystals and interstitial glass (crosses). A SEM image (upper right) shows dark grey glass rimmed by a zone with light grey quench crystals. Bright spots are holes (blue arrows) due to edge effect. Symbols with the same colors are analyses of the same inclusions. Note that both outer zones and central glass pools have identical bulk compositions, indicating that crystallization of the outer zone did not affect the composition of the remaining melt in the core.

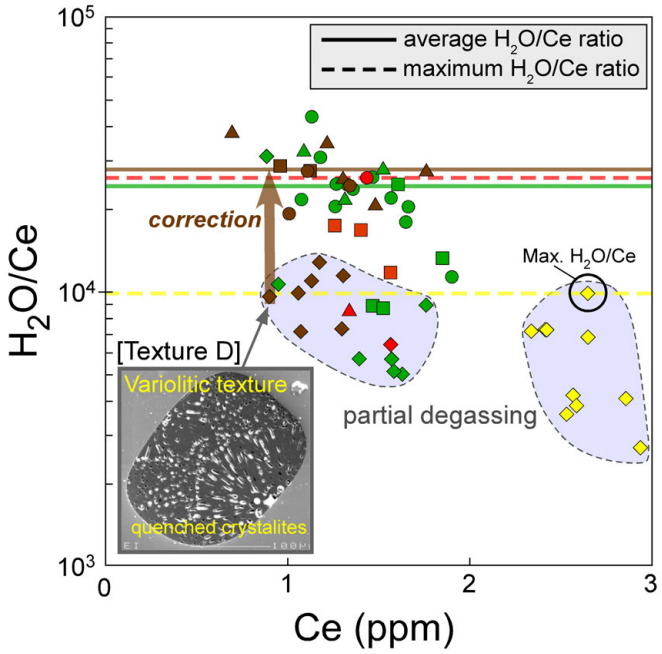

Figure DR-4. H_2O/Ce plotted against Ce of melt inclusions of high-Si-D (green) and high-Si-V (brown), and low-Si-D (red) and low-Si-F (yellow). Variolitic inclusions (solid diamonds) (Figs. 1D, DR-2D) have consistently lower H_2O/Ce ratios compared to glass in melt inclusions comprising pure glass and a few shrinkage vesicles (circles, squares and triangles) (Figs. 1A, 1B, 1C, DR-2A, 2B, 2C) of the same geochemical type. These variolitic inclusions are considered to have partly lost their water upon entrapment due to degassing. For these inclusions, the original water contents were restored based on Ce contents, by assuming the original H_2O/Ce ratios of the variolitic samples to be equal to the average H_2O/Ce ratio of undegassed samples of the same geochemical type.

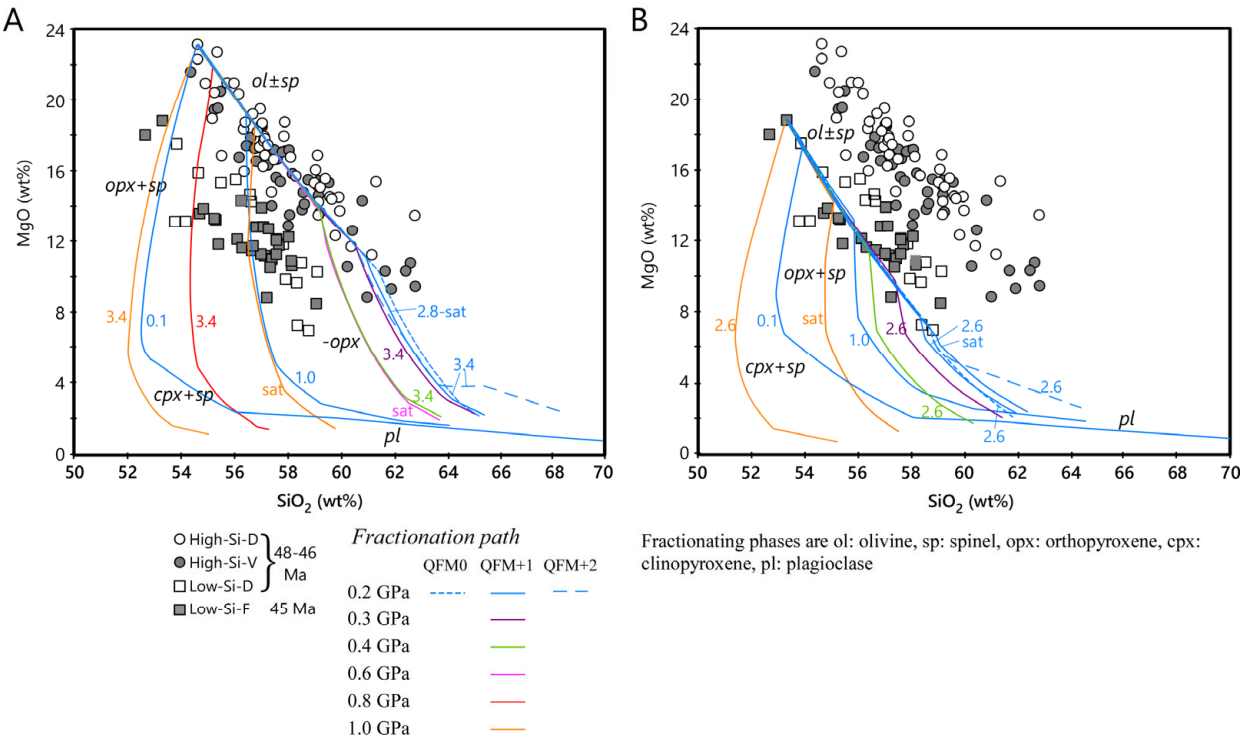

Figure DR-5. Examples of fractional crystallization paths for primary boninite magmas of the high-Si-D (A) and the low-Si-F (B) by alphaMELTS (Smith and Asimow, 2005), compared with boninitic melt inclusions (circles and squares). The numbers beside the paths are H_2O contents (wt%) in the primary magmas. Calculations were done under fO_2 of Δlog(FMQ)=+1 at pressures 0.2-1.0 GPa, and also under fO_2 of Δlog(FMQ)=0 and +2 at 0.2 GPa. Change in fO_2 by 2 log units only slightly shifts the fractionation paths. The high-Si boninitic inclusions are mostly plot around low-P (<0.4 GPa), high-H_2O (>2.8 wt%) paths. Higher pressure or lower H_2O content leads to earlier crystallization of orthopyroxene and rapid decreases of MgO, away from the clusters of melt inclusion compositions. The variation of the low-Si inclusions also consistent with low-P (<0.3 GPa), high-H_2O (>2.6 wt%) conditions, suggesting minimal H_2O loss during fractionation. Those plotted at higher MgO than the olivine-fractionation paths suggest mixing of relatively primitive and differentiated melts.

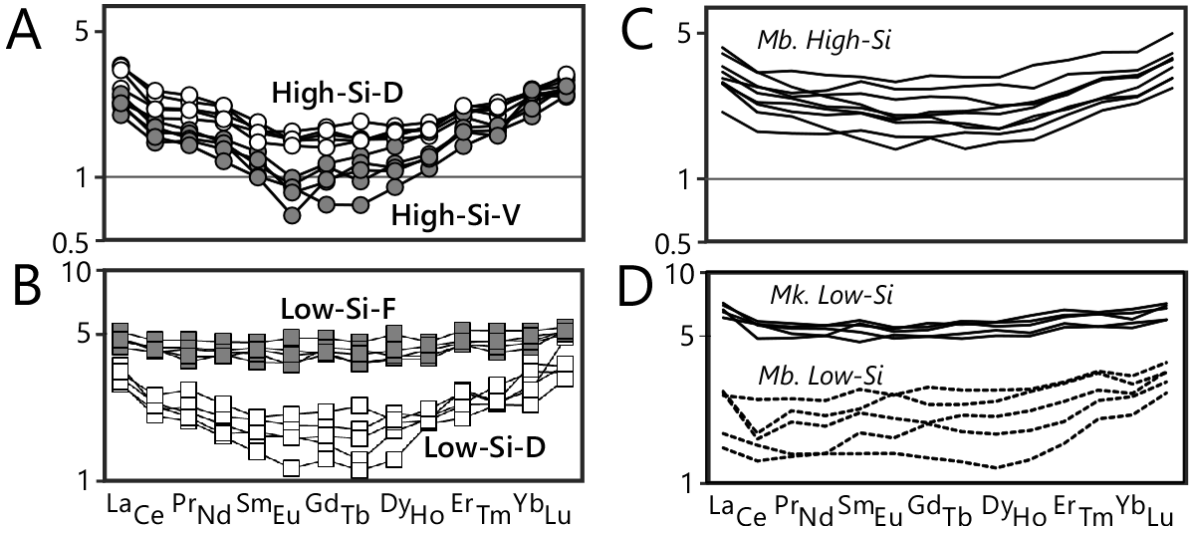

Figure DR-6. Chondrite-normalized REE patterns for the high-Si-D and high-Si-V (A) and the low-Si-D and low-Si-F (B) melt inclusions, compared with the whole-rock compositions (after Kanayama et al., 2012) of high-Si boninite from the 48-46 Ma Maruberiwan Formation (Mb.) (C), and those of low-Si boninites from the 45-Ma Mikazukiyama (Mk.) and 48-46 Ma Maruberiwan (Mb.) Formation (D).

TABLE DR-1. REPRESENTATIVE ANALYSES OF MELT INCLUSIONS IN CHROME SPINEL AND THE ESTIMATED T-P CONDITIONS FOR THE PRIMARY BONINITES

Formation	Maruberiwan												Mikazukiyama			
Geochem.Type	High-Si-V*	High-Si-V	High-Si-V	High-Si-V	High-Si-D*	High-Si-D	High-Si-D	High-Si-D	Low-Si-D*	Low-Si-D	Low-Si-D	Low-Si-D	Low-Si-F*	Low-Si-F	Low-Si-F	Low-Si-F
No. of analyses	3	3	2	3	3	3	3	2	1	2	3	3	5	3	5	2
SiO_2	52.63 ± 0.27	55.89 ± 0.41	58.38 ± 0.51	58.36 ± 0.08	52.20 ± 0.54	56.09 ± 0.42	56.43 ± 0.16	54.95 ± 0.06	53.53 ± 0.22	54.91 ± 0.68	56.12 ± 0.31	57.34 ± 0.17	51.38 ± 0.89	57.75 ± 0.45	53.48 ± 0.31	54.30 ± 0.88
TiO_2	0.09 ± 0.03	0.08 ± 0.05	0.06 ± 0.00	0.07 ± 0.04	0.06 ± 0.02	0.09 ± 0.03	0.08 ± 0.03	0.05 ± 0.04	0.14 ± 0.01	0.10 ± 0.03	0.10 ± 0.04	0.14 ± 0.03	0.12 ± 0.04	0.16 ± 0.04	0.19 ± 0.04	0.13 ± 0.03
Al_2O_3	7.70 ± 0.09	8.16 ± 0.06	10.77 ± 0.14	8.62 ± 0.04	6.42 ± 0.11	7.37 ± 0.15	6.87 ± 0.04	7.10 ± 0.07	10.73 ± 0.10	9.03 ± 0.03	10.05 ± 0.10	11.67 ± 0.07	8.81 ± 0.33	11.58 ± 0.22	10.69 ± 0.33	10.56 ± 0.29
FeO*	8.29 ± 0.16	8.21 ± 0.06	6.49 ± 0.11	7.60 ± 0.20	9.11 ± 0.57	9.19 ± 0.21	8.50 ± 0.17	8.36 ± 0.27	6.37 ± 0.18	10.02 ± 0.04	8.97 ± 0.14	8.20 ± 0.05	8.61 ± 0.26	7.24 ± 0.51	9.41 ± 0.45	6.27 ± 0.32
MnO	0.23 ± 0.05	0.14 ± 0.02	0.19 ± 0.03	0.19 ± 0.05	0.16 ± 0.03	0.23 ± 0.07	0.19 ± 0.03	0.19 ± 0.02	0.10 ± 0.02	0.17 ± 0.05	0.16 ± 0.03	0.13 ± 0.05	0.18 ± 0.08	0.10 ± 0.03	0.24 ± 0.07	0.24 ± 0.08
MgO	20.90 ± 0.63	16.69 ± 0.08	9.76 ± 0.06	15.02 ± 0.11	22.12 ± 0.50	15.1 ± 0.24	18.26 ± 0.11	18.79 ± 0.06	17.41 ± 0.14	15.19 ± 0.10	14.13 ± 0.12	9.49 ± 0.06	18.12 ± 0.66	8.29 ± 0.42	13.52 ± 0.91	10.38 ± 0.68
CaO	5.24 ± 0.12	6.24 ± 0.07	6.93 ± 0.03	6.21 ± 0.10	4.33 ± 0.09	6.25 ± 0.10	5.14 ± 0.03	5.04 ± 0.13	9.02 ± 0.10	6.03 ± 0.04	7.13 ± 0.07	8.34 ± 0.06	7.47 ± 0.31	10.51 ± 0.25	7.97 ± 0.23	9.99 ± 0.35
Na_2O	0.71 ± 0.05	1.25 ± 0.08	1.54 ± 0.00	1.32 ± 0.02	0.33 ± 0.02	1.21 ± 0.03	0.99 ± 0.03	1.27 ± 0.04	0.65 ± 0.04	1.12 ± 0.08	1.38 ± 0.06	1.65 ± 0.04	0.97 ± 0.09	1.48 ± 0.10	1.15 ± 0.09	1.27 ± 0.13
K_2O	0.39 ± 0.06	0.35 ± 0.03	0.26 ± 0.00	0.43 ± 0.01	0.38 ± 0.02	0.31 ± 0.03	0.24 ± 0.05	0.38 ± 0.04	0.16 ± 0.01	0.35 ± 0.04	0.41 ± 0.01	0.39 ± 0.01	0.32 ± 0.05	0.34 ± 0.01	0.32 ± 0.03	0.33 ± 0.05
Cr_2O_3	0.62 ± 0.09	0.19 ± 0.04	0.28 ± 0.05	0.19 ± 0.05	0.45 ± 0.06	0.35 ± 0.06	0.77 ± 0.04	0.31 ± 0.06	1.31 ± 0.05	1.02 ± 0.10	0.65 ± 0.04	0.93 ± 0.02	0.37 ± 0.04	0.31 ± 0.10	0.54 ± 0.07	1.11 ± 0.03
H_2O	2.5 ± 0.5	1.9 ± 0.3	2.8 ± 0.1	3.1 ± 0.1	3.4 ±0.6	3.2 ± 1.6	2.3 ± 0.2	2.1 ± 0.5	2.1±0.1	1.8 ± 0.1	2.2 ± 0.3	1.8 ± 0.3	2.6±0.7	1.2 ± 0.1	2.1 ± 0.3	1.2 ± 0.1
Total	96.81 ± 0.93	97.19 ± 0.34	94.67 ± 0.65	98.01 ± 0.22	95.55 ± 0.96	96.19 ± 0.56	97.47 ± 0.14	96.43 ± 0.21	99.41 ± 0.89	97.94 ± 0.56	99.09 ± 0.33	98.28 ± 0.25	96.37 ± 1.63	97.76 ± 0.41	97.50 ± 1.43	94.56 ± 0.08
$Fe^{3+}/\Sigma Fe$	0.09-0.20				0.09-0.20				0.11-0.24				0.10-0.22			
°C	1423-1428				1415-1419				1343-1347				1378-1384			
GPa	0.89-0.96				0.74-0.80				0.54-0.59				0.81-0.88			
Fo	95.0-95.8				94.4-95.3				95.7-96.4				94.0-95.2			
Tace element compositions [μg/g]																
Li	5.73	7.75		7.27	27.02	5.77	7.20	9.17			6.87	8.81	5.09	5.03	5.09	4.17
B	8.15	10.54		15.82	4.62	10.94	9.08	4.09	10.05		13.52	11.78	6.55	6.57	6.55	8.49
Sc	35.57	33.54		32.98	26.70	31.67	29.81	28.42	51.71		43.12	42.25	56.59	47.19	56.59	45.64
Ti	335.77	409.02		437.78	392.14	534.31	466.18	399.03	624.10		508.74	738.16	1396.72	1214.67	1396.72	866.92
V	159.28	157.75		169.12	134.30	238.77	153.21	141.60	412.26		241.23	244.42	264.64	212.18	264.64	131.51
Co	61.65	54.87		47.33	72.58	59.56	63.84	66.84	96.43		51.21	47.45	49.71	36.89	49.71	31.70
Ni	397.66	259.95		167.02	363.20	108.96	251.07	283.56	233.43		139.76	100.60	132.83	83.60	132.83	84.28
Rb	11.67	11.60		15.21	9.68	9.39	7.01	11.38	7.34		13.35	12.60	5.21	5.05	5.21	5.71
Sr	29.54	39.46		43.52	44.50	60.53	51.22	58.17	53.36		52.24	71.98	93.20	101.86	93.20	103.34
Y	2.04	2.58		2.40	2.86	2.74	3.12	2.90	2.24		2.57	3.36	5.99	7.35	5.99	6.23
Zr	11.72	13.83		16.63	15.15	13.28	14.92	15.93	9.27		13.69	18.76	16.78	17.12	16.78	17.17
Nb	0.31	0.31		0.37	0.38	0.26	0.17	0.52	0.73		0.33	0.42	0.53	0.56	0.53	1.14
Cs	25.66	0.58		0.61	17.52	0.36	0.23	0.54			0.60	0.65	0.18	0.18	0.18	3.96
Ba	27.69	26.83		32.19	13.87	31.11	23.28	40.27	21.08		28.67	33.79	34.98	36.63	34.98	40.23
La	0.47	0.52		0.56	0.69	0.64	0.50	0.97	0.54		0.69	0.78	1.12	1.22	1.12	1.92
Ce	0.90	1.01		1.12	1.39	1.32	1.08	1.83	0.82		1.25	1.57	2.65	2.86	2.65	5.88
Pr	0.14	0.15		0.17	0.23	0.20	0.16	0.27	0.12		0.18	0.25	0.40	0.43	0.40	0.53
Nd	0.62	0.70		0.72	1.13	0.92	0.79	1.19	0.80		0.74	1.06	1.90	2.10	1.90	1.89
Sm	0.18	0.20		0.21	0.31	0.25	0.24	0.33			0.20	0.30	0.64	0.67	0.64	0.47
Eu	0.05	0.06		0.06	0.11	0.08	0.11	0.11	0.09		0.06	0.12	0.23	0.27	0.23	0.19
Gd	0.19	0.23		0.24	0.41	0.32	0.38	0.35	0.35		0.25	0.42	0.80	0.95	0.80	0.78
Tb	0.04	0.05		0.04	0.08	0.06	0.05	0.07			0.04	0.08	0.13	0.16	0.13	0.12
Dy	0.27	0.35		0.31	0.47	0.39	0.44	0.43	0.47		0.31	0.48	0.95	1.23	0.95	1.03
Ho	0.07	0.09		0.08	0.10	0.10	0.08	0.13			0.10	0.12	0.23	0.25	0.23	0.22
Er	0.28	0.33		0.28	0.37	0.34	0.33	0.32	0.36		0.32	0.42	0.73	0.83	0.73	0.70
Tm	0.04	0.05		0.05	0.05	0.05	0.07	0.05			0.06	0.06	0.12	0.13	0.12	0.10
Yb	0.35	0.43		0.36	0.44	0.40	0.40	0.41	0.41		0.37	0.44	0.74	0.83	0.74	0.70
Lu	0.07	0.08		0.07	0.08	0.07	0.07	0.07	0.07		0.07	0.12	0.13	0.13	0.13	0.13
Hf	0.31	0.37		0.45	0.52	0.38	0.40	0.49	0.44		0.47	0.61	0.46	0.50	0.46	0.59
Ta	0.03	0.02		0.02	0.03	0.02		0.03			0.02	0.02	0.03	0.03	0.03	0.07
Pb	1.66	1.39		1.20	1.70	1.50	0.99	1.64	1.02		1.13	1.59	1.07	1.05	1.07	0.87
Th	0.08	0.07		0.06	0.14	0.10	0.06	0.12			0.08	0.10	0.13	0.15	0.13	0.14
U	0.08	0.08		0.07	0.12	0.10	0.07	0.14			0.09	0.08	0.09	0.10	0.09	0.18

Major element oxides are listed in wt%. 1σ of major element oxides are standard deviations of multiple analyses, except the primary Low-Si-D melt inclusion (*) for which 1σ is given as statistic errors of X-ray count.

Primary boninite compositions of the four geochemical types are denoted by asterisks (*) and are listed with the estimated T-P conditions and Fo contents at olivine and orthopyroxene multiple saturation.

Considering the uncertainties of H_2O contents and f_{O2}, T-P estimates are shown as ranges including 1σ of H_2O and f_{O2} of ΔFMQ 1±1 in log unit.

Table DR-2. Repeated analyses of standard glass NIST610, NIST612, and BIR. Reference values are from Jochum and Nohl (2008).

NIST610	Li	B	Sc	Ti	V	Co	Ni	Rb	Sr	Y	Zr	Nb	Cs	Ba	La	Ce	Pr	Nd	Sm	Eu	Gd	Tb	Dy	Ho	Er	Tm	Yb	Lu	Hf	Ta	Pb	Th	U
Reference value [μg/g]	485	356	441	434	442	405	444	431	497	450	440	419	361	424	457	448	430	431	451	461	420	443	427	449	426	420	462	435	418	377	413	451	457
Average of 24 anal. [μg/g]	491	250	511	502	488	445	405	454	579	584	537	506	405	489	500	519	517	500	525	508	533	549	533	558	558	528	546	551	521	532	463	528	508
Standard deviation [μg/g]	17	61	36	18	12	11	24	9	27	55	42	19.2	10.2	15.0	27.3	16.3	23.3	27.7	31.2	29.9	40.5	50.0	48.3	53.9	51.8	59.0	48.5	62.0	54.9	35.9	12.9	44.2	13.8
RSD (%)	3.4	24.2	7.0	3.6	2.5	2.5	6.0	2.0	4.7	9.4	7.9	3.8	2.5	3.1	5.5	3.1	4.5	5.5	5.9	5.9	7.6	9.1	9.1	9.7	9.3	11.2	8.9	11.3	10.5	6.7	2.8	8.4	2.7
Accuracy (%)	1.4	-42.5	13.7	13.6	9.4	9.0	-9.7	5.1	14.1	23.0	18.0	17.1	10.8	13.3	8.6	13.8	16.8	13.8	14.1	9.2	21.3	19.3	19.9	19.4	23.7	20.4	15.4	21.1	19.9	29.2	10.8	14.7	10.0

NIST612	Li	B	Sc	Ti	V	Co	Ni	Rb	Sr	Y	Zr	Nb	Cs	Ba	La	Ce	Pr	Nd	Sm	Eu	Gd	Tb	Dy	Ho	Er	Tm	Yb	Lu	Hf	Ta	Pb	Th	U
Reference value [μg/g]	42	43	44	45	46	47	48	49	50	51	52	53	54	55	56	57	58	59	60	61	62	63	64	65	66	67	68	69	70	71	72	73	74
Average of 9 anal. [μg/g]	42	26	41	43	41	40	36	33	84	44	42	40	46	41	38	43	41	39	41	38	41	43	41	42	44	42	43	42	41	42	43	41	41
Standard deviation [μg/g]	1	2	0	1	0	0	1	0	1	1	1	0.6	0.7	0.3	0.6	0.3	0.4	0.3	0.3	0.4	0.7	0.5	0.7	1.1	1.2	0.6	0.6	0.7	0.1	0.0	0.4	0.3	0.4
RSD (%)	2.5	6.2	1.1	2.2	0.9	0.8	3.5	1.5	0.9	2.0	2.3	1.5	1.6	0.6	1.6	0.8	1.0	0.9	0.7	1.1	1.7	1.2	1.8	2.6	2.7	1.5	1.4	1.6	0.2	0.0	0.9	0.7	1.1
Accuracy (%)	1.0	-63.2	-5.8	-3.5	-10.2	-16.5	-31.9	-46.0	41.0	-14.3	-21.8	-31.9	-16.8	-32.2	-45.3	-32.4	-39.3	-50.2	-46.4	-60.6	-51.4	-45.6	-55.6	-51.9	-50.5	-58.8	-57.7	-62.2	-70.3	-66.7	-66.4	-77.6	-79.4

BIR-1G	Li	B	Sc	Ti	V	Co	Ni	Rb	Sr	Y	Zr	Nb	Cs	Ba	La	Ce	Pr	Nd	Sm	Eu	Gd	Tb	Dy	Ho	Er	Tm	Yb	Lu	Hf	Ta	Pb	Th	U
Reference value [μg/g]	3		43	5400	326	52	178	0.2	109	14	14	0.52	0.01	6.50	0.61	1.89	0.37	2.37	1.09	0.52	1.85	0.35	2.55	0.56	1.70	0.24	1.64	0.25	0.57	0.04	3.70	0.03	0.02
Average of 13 anal. [μg/g]	3	2	41	5740	327	54	143	0	110	14	14	1	0	7	1	2	0	2	1	1	2	0	2	1	2	0	2	0	1	0	4	0	0
Standard deviation [μg/g]	0	1	1	114	8	1	12	0	3	0	0	0	0	0	0	0	0	0	0	0	0	0	0	0	0	0	0	0	0	0	0	0	0
RSD (%)	3.1	53.0	2.3	2.0	2.3	2.0	8.5	5.5	2.4	3.0	2.5	6.2	71.4	3.7	4.5	3.1	4.2	4.4	3.4	3.8	4.2	6.8	5.0	6.2	3.5	5.6	5.0	9.0	8.4	27.9	3.7	16.9	30.8
Accuracy (%)	-0.7		-4.4	5.9	0.4	4.5	-24.3	-0.3	0.8	0.2	-2.9	-1.9	-36.8	1.4	-3.3	3.8	0.3	-1.0	-0.2	0.1	-9.0	-2.9	-2.9	-5.7	-4.8	-3.2	-2.3	-7.3	-3.8	3.2	-3.4	-6.2	-37.2